

Nematic liquid-crystal alignment on stripe-patterned substrates

ANQUETIL-DECK, Candy and CLEAVER, Doug <<http://orcid.org/0000-0002-4278-0098>>

Available from Sheffield Hallam University Research Archive (SHURA) at:
<http://shura.shu.ac.uk/2996/>

This document is the author deposited version. You are advised to consult the publisher's version if you wish to cite from it.

Published version

ANQUETIL-DECK, Candy and CLEAVER, Doug (2010). Nematic liquid-crystal alignment on stripe-patterned substrates. *Physical Review E (PRE)*, 82 (3), 031709.

Copyright and re-use policy

See <http://shura.shu.ac.uk/information.html>

Nematic Liquid Crystal Alignment on Stripe Patterned Substrates

C. Anquetil-Deck

*Laboratoire Chimie Provence, UMR 6264 University of Aix-Marseille I,
Avenue Escadrille Normandie-Niemen, 13397 Marseille Cedex 20, France*

D.J. Cleaver*

*Materials and Engineering Research Institute, Sheffield Hallam University,
City Campus, Howard Street, Sheffield, S1 1WB, UK*

(Dated: August 13, 2010)

Here, we use molecular simulation to consider the behaviour of a thin nematic film confined between two identical nano-patterned substrates. Using patterns involving alternating stripes of homeotropic-favouring and homogeneous-favouring substrate, we investigate the influence of the relative stripe width and the film thickness. From this, we show that the polar anchoring angle can be varied continuously from planar to homeotropic by appropriate tuning of these parameters. For very thin films with equal stripe widths, we observe orientational bridging, the surface patterning being written in domains which traverse the nematic film. This dual-bridging-domain arrangement breaks down with increase in film thickness, however, being replaced by a single tilted monodomain. Strong azimuthal anchoring in the plane of the stripe boundaries is observed for all systems.

I. INTRODUCTION

The means by which the director orientation of a bulk liquid crystal (LC) is imposed by its confining substrates is called anchoring [1]. The vast majority of LC switching devices rely in some way on anchoring to set their dynamic and equilibrium properties. Substrate-controlled director alignment is a device-scale effect which results from the interplay of the microscopic orientational and positional degrees of freedom of the LC molecules located in the proximity of their confining surfaces. Traditional routes to establishing desired anchoring behaviours include substrate rubbing and various photoalignment approaches such as light-induced cis-trans isomerisation and photodegradation. The molecular mechanisms by which these operate are, though, poorly understood.

More recently, developments have been made in utilising spatially inhomogeneous substrates to control LC anchoring properties. The most obvious systems that fall into this category are the structurally inhomogeneous substrates employed in the zenithally bistable nematic [2] and post-aligned bistable nematic [3] device geometries. In these, long-lived bistability is achieved due to the ability of the structured substrates to stabilise optically distinct continuous and defect states. An alternative, but monostable, alignment approach based on steric patterning utilises regular scratch arrays, etched using atomic force microscope tips [4].

Chemical patterning offers an alternative approach by which to impose substrate inhomogeneity in LC systems. The concept of simultaneous alignment of azimuthal and

polar orientation of LCs by chemical nanopatterns has also been suggested experimentally [5–7]. In 2005, Scharf *et al.* [8, 9] discussed the alignment properties of nematic LCs on surfaces containing homeotropic and planar alignment areas on the same substrate. They showed that the polar orientation depends on the ratio of the homeotropic/planar surface potential areas, while the LC azimuthally orients along the direction of the stripes [10]. Alternative systems utilising alkanethiol Self Assemble Monolayers (SAMs) on gold have been developed by the groups of Abbott [11] and Evans [12]. Using microcontact printing, these systems are able to achieve highly reproducible surface features with periodicities of 10s of microns. Square, circular and stripes patterns written on these lengthscales have, thus, been observed using optical microscopy in crossed polariser set-ups. An alternative approach, employing selective ultra-violet irradiation of SAMs, has achieved LC-aligning stripe patterns on the sub-micron scale [13].

In Ref [14], we contributed the simulation aspects of a joint experimental / simulation study of LC alignment at a single patterned substrate. In this, it was shown that a range of patterned SAMs can be used to control LC alignment states and domains. For stripe patterns, the LC was found to align parallel to the stripe boundaries for both nanoscale simulation features and micron-scale experimental systems. Indeed, despite the significantly different length-scales involved, the qualitative behaviour seen in MC simulations of generic molecular models confined using a striped interface proved entirely consistent with the experimental observations. Specifically, on undergoing isotropic to nematic ordering, all systems proved to be dominated by the homeotropic-aligning substrate regions at the ordering transition, the influence of the planar-aligning regions only becoming apparent well into the nematic.

*Electronic address: d.j.cleaver@shu.ac.uk

In this paper, we follow up on our previous single-patterned substrate results by concentrating on the behaviour of confined LC films systems with stripe patterns on both of their substrates and study the influence of the film thickness and the relative proportions of homeotropic and planar alignment areas on the substrates. In section II we present our model system and describe the simulation methodology employed. Section III contains results obtained from an initial thin-film system with equal stripe widths. In Sections IV and V, respectively, we examine the influence of relative stripe width and of film thickness. Finally, in Section VI, we draw some conclusions.

II. MODEL AND SIMULATION DETAILS

We have performed a series of Monte Carlo (MC) simulations of rod-shaped particles confined in slab geome-

try between two planar walls. Inter-particle interactions have been modelled through the Hard Gaussian Overlap (HGO) potential [15]. Here, the dependence of the interaction potential ν^{HGO} on $\hat{\mathbf{u}}_i$ and $\hat{\mathbf{u}}_j$, the orientations of particles i and j , and $\hat{\mathbf{r}}_{ij}$, the inter-particle unit vector is

$$\nu^{HGO} = \begin{cases} 0 & \text{if } r_{ij} \geq \sigma(\hat{\mathbf{r}}_{ij}, \hat{\mathbf{u}}_i, \hat{\mathbf{u}}_j) \\ \infty & \text{if } r_{ij} < \sigma(\hat{\mathbf{r}}_{ij}, \hat{\mathbf{u}}_i, \hat{\mathbf{u}}_j) \end{cases}$$

where $\sigma(\hat{\mathbf{r}}_{ij}, \hat{\mathbf{u}}_i, \hat{\mathbf{u}}_j)$, the contact distance, is given by

$$\sigma(\hat{\mathbf{r}}_{ij}, \hat{\mathbf{u}}_i, \hat{\mathbf{u}}_j) = \sigma_0 \left[1 - \frac{\chi}{2} \left[\frac{(\hat{\mathbf{r}}_{ij} \cdot \hat{\mathbf{u}}_i + \hat{\mathbf{r}}_{ij} \cdot \hat{\mathbf{u}}_j)^2}{1 + \chi(\hat{\mathbf{u}}_i \cdot \hat{\mathbf{u}}_j)} + \frac{(\hat{\mathbf{r}}_{ij} \cdot \hat{\mathbf{u}}_i - \hat{\mathbf{r}}_{ij} \cdot \hat{\mathbf{u}}_j)^2}{1 - \chi(\hat{\mathbf{u}}_i \cdot \hat{\mathbf{u}}_j)} \right] \right]^{-1/2}. \quad (1)$$

The parameter χ is set by the particle length to breadth ratio $\kappa = \sigma_{end}/\sigma_{side}$ via

$$\chi = \frac{\kappa^2 - 1}{\kappa^2 + 1}. \quad (2)$$

Particle-substrate interactions have been modelled using the hard needle-wall potential (HNW) [16]. In this, the particles do not interact directly with the surfaces. Rather the surface interaction is achieved by considering a hard axial needle of length $\sigma_0 k_s$ placed at the centre of each particle (see Figure 1). This gives an interaction

$$\nu^{HNW} = \begin{cases} 0 & \text{if } |z_i - z_0| \geq \sigma_w(\hat{\mathbf{u}}_i) \\ \infty & \text{if } |z_i - z_0| < \sigma_w(\hat{\mathbf{u}}_i) \end{cases}$$

where z_0 represents the location of a substrate and

$$\sigma_w(\hat{\mathbf{u}}_i) = \frac{1}{2} \sigma_0 k_s \cos(\theta_i) \quad (3)$$

Here, k_s is the dimensionless needle length and $\theta_i = \arccos(u_{i,z})$ is the angle between the substrate normal and the particle's orientation vector. For small k_s , the homeotropic arrangement has been shown to be stable, whereas planar anchoring is favoured for long k_s [16]. Furthermore, despite its simplicity, the HNW potential has been found to exhibit qualitatively identical behaviour to that obtained using more complex particle-substrate potentials [17]. Here, by imposing variation in k_s across the two boundary walls, we investigate the

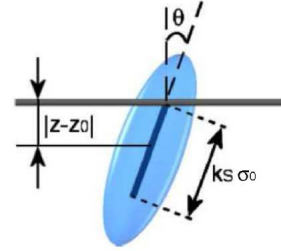


FIG. 1: (Color online) Schematic representation of the geometry used for the hard needle-wall (HNW) particle-substrate interaction [16].

effects of molecular-scale substrate patterning on LC anchoring. The results presented in Sections III and IV have been obtained for systems of 864, $\kappa = 3$ HGO particles confined between two stripe patterned substrates. In these systems, the substrates were separated by a distance $L_z = 4\kappa\sigma_0$, periodic boundary conditions being imposed in the x - and y -directions.

On each substrate, k_s was set to a homeotropic-aligning value ($k_s = 0$) for a stripe portion of its area and a planar value ($k_s = 3$) for the remainder. Here, sharp boundaries have been imposed between the different alignment regions, the stripe boundaries running parallel to the y -axis of the simulation box. The patterns on the top and

bottom surfaces have been kept in perfect registry with one another, as shown in the schematic diagram 2. Each system has been initialised at low density and gently compressed by decreasing the box dimensions L_x and L_y . At each density, run lengths of 1 million MC sweeps (where one sweep represents one attempted move per particle) were performed, averages and profiles being accumulated for the final 500 000 sweeps.

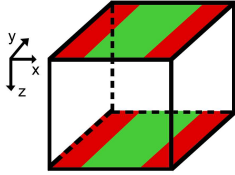


FIG. 2: (Color online) Schematic representation of stripe patterned systems with alternating homeotropic-inducing (red/dark) and planar-inducing (green/light) substrate regions.

Detailed analysis was performed by dividing stored system configurations into 100 equidistant constant- z slices and calculating averages of relevant observables in each slice. This yielded profiles of quantities, such as number density, $\rho^*(z)$, from which structural changes could be assessed. Orientational order profiles were also measured, particularly

$$Q_{zz}(z) = \frac{1}{N(z)} \sum_{i=1}^{N(z)} \left(\frac{3}{2} u_{i,z}^2 - \frac{1}{2} \right) \quad (4)$$

which measures variation across the confined films of orientational order measured with respect to the substrate normal. Here $N(z)$ is the instantaneous occupancy of the relevant slice. We have also further subdivided the system to assess lateral inhomogeneities induced by the patterning.

III. INITIAL STRIPE-PATTERNED SYSTEM

In the first system considered here, the proportions of the homeotropic and planar alignment regions were both set to 50%. The outcomes of these first striped system simulations are summarised by the snapshots shown in Figs. 3. Several remarks emerge from these. At low density ($\rho^* = 0.3$), the central region of the film remains relatively disordered, but the near-surface regions adopt orientations consistent with their imposed k_s values (Fig. 3(a)). Even at the relatively low density of $\rho^* = 0.32$, the particles adjacent to the $k_s = 3$ stripes

show a marked preference to lie parallel to the stripe boundaries (Fig. 3(b)). With increase in density, orientational order appears to develop between the $k_s=0$ surface regions (Fig. 3(c)) while the other central region of the film (confined between $k_s = 3$ substrate regions) remains relatively disordered. At the reduced density $\rho^* = 0.39$ (Fig. 3(e)), both mid-film regions appear orientationally ordered. However, rather than forming a monodomain, the orientations adopted in the two central regions are apparently the same as those of the particles aligned at the corresponding substrate regions: the stripe pattern is, thus, written across the film in domains, in an interesting manifestation of bridging [18, 19].

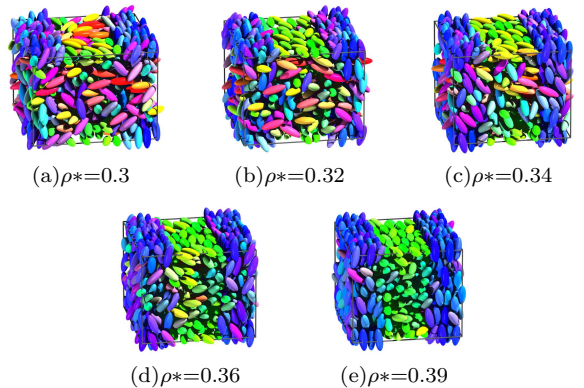
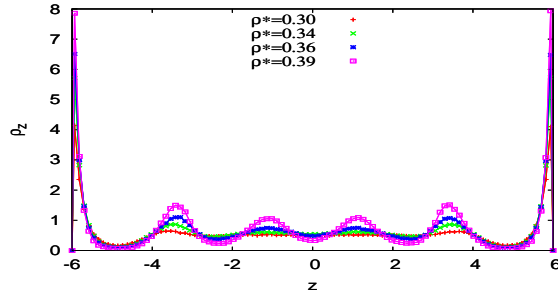
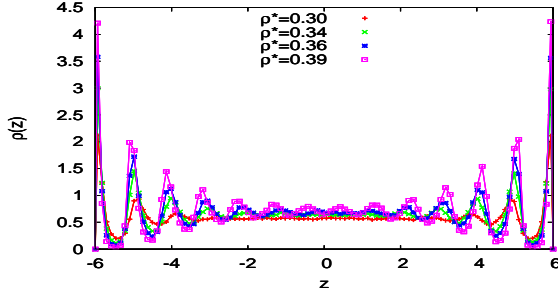


FIG. 3: (Color online) Snapshots of the 50-50 stripe patterned system at a series of reduced densities. Colour coding is used to indicate particle orientation

In the light of these observations, we have analysed the behaviour of this system by calculating pairs of profiles of key observables, the simulated system being split in two according to the imposed substrate pattern - for analysis purposes, particles are allocated to homeotropic-confined or homogeneous-confined regions according to their x -coordinates. Whilst there is further x -dependence within these two regions, we have found that the dominant inhomogeneity is the discontinuity apparent from Figs. 3.

The density profile depicted in Fig. 4(a) shows adsorption characteristics for the portion of the film confined between the homeotropic substrate regions. This shows that increasing the density leads to formation of surface layers with a periodicity of $\simeq 2.5\sigma_0$. This distance corresponds approximately to the particle length. Fig. 4(b) shows that, in the planar-confined part of the film, conversely, the layers formed have a periodicity of about σ_0 . In this region, then, it appears that the molecules are arranged side to side close to the substrates but that the positional structure is smeared out in the central region.

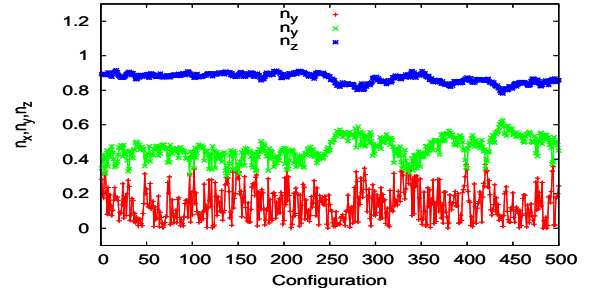
To characterise this behaviour further, we have calculated the average director for particles in the central 50%

(a) $\rho_l(z)$ profile for the homeotropic-confined region(b) $\rho_l(z)$ profile for the planar-confined regionFIG. 4: (Color online) Density profiles for the 50:50 stripe patterned system at different average densities ρ^* .

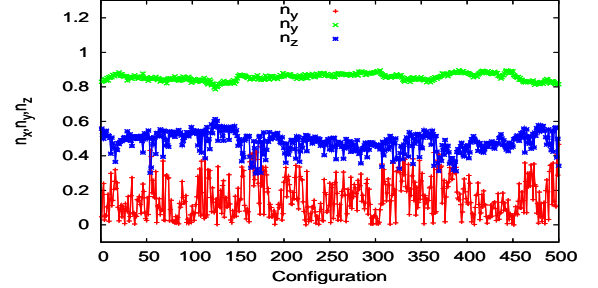
of each half of our system. We denote the director components along the simulation box axes as n_x , n_y and n_z . The angles θ_x , θ_y and θ_z formed between the box axes and the director can then be readily determined by inversion of these direction cosines. Characteristic behaviour of the two sets of n_x , n_y and n_z is shown on Fig. 5 as simulation 'time'-series calculated for 500 configurations in the production sequence of the $\rho^* = 0.4$ run.

Fig. 5(a) shows that the portion of the film subjected to homeotropic alignment has its largest director component aligned along the z -axis, apparently, corresponding to homeotropic anchoring. In the other portion of the film, conversely, the largest component is aligned along the y -direction (Fig. 5(b)). To determine the tilt angles in the two regions, we use the angle measured with respect to the largest component in each region, since this suffers least from noise. From this, we obtain angles of $\theta_z = 29^\circ$ in the homeotropic-confined region and $\theta_y = 28^\circ$ in the planar-confined region. These director tilt angles are significantly different from one another but are also very different from the zero values expected for classic homeotropic and planar anchoring. Thus, they indicate the initial inference drawn from the snapshots Figs. 3, that the confined film is split into homeotropic and planar portions, may not be fully correct.

A more complete understanding of the orientational aspects of the surface induced ordering in this system can



(a) Homeotropic-confined region



(b) Planar-confined region

FIG. 5: (Color online) 'Time' series showing the director components for 500 configuration in the $\rho^* = 0.4$ production run.

be obtained from profiles of the three diagonal order tensor components Q_{ii} . For perfect homeotropic anchoring, Q_{zz} should tend to 1, with Q_{xx} and Q_{yy} going to -0.5. At low density, Figs. 6 show that both Q_{xx} and Q_{yy} are negative close to the homeotropic wall regions. On increasing the density, peaks appear in the bulk region and Q_{xx} drops to -0.4. However, the value of Q_{yy} stagnates at around -0.1. Fig. 6(c) shows that, at low density, the corresponding Q_{zz} profile is zero in the mid-film region but positive close to the substrates, consistent with homeotropic order developing at the walls. On increasing the density, the mid-film Q_{zz} value increases, indicating onset of orientational order with significant alignment along the z -axis. The average mid-film Q_{zz} value fails to exceed 0.5 at high densities, however. These profiles indicate, therefore, that the mid-film director has homeotropic character but, because the Q_{yy} value is well above -0.5, it is tilted in the yz -plane.

In the planar-confined region, the behaviour of these diagonal order tensor components shows some marked differences. At low density, Q_{xx} (Fig. 7(a)) is zero everywhere. As the density is increased, however, Q_{xx} rapidly becomes negative close to the walls and subsequently goes negative across the whole of the film. Thus, at high density ($\rho^* = 0.38$), Q_{xx} is about -0.4 throughout. This indicates strong particle alignment perpendicular to the x -axis, i.e. in the plane of the stripe boundaries. At low density, Q_{yy} (Fig. 7(b)) is positive close to the walls (~ 0.5) and zero in the mid-film region. As the density is

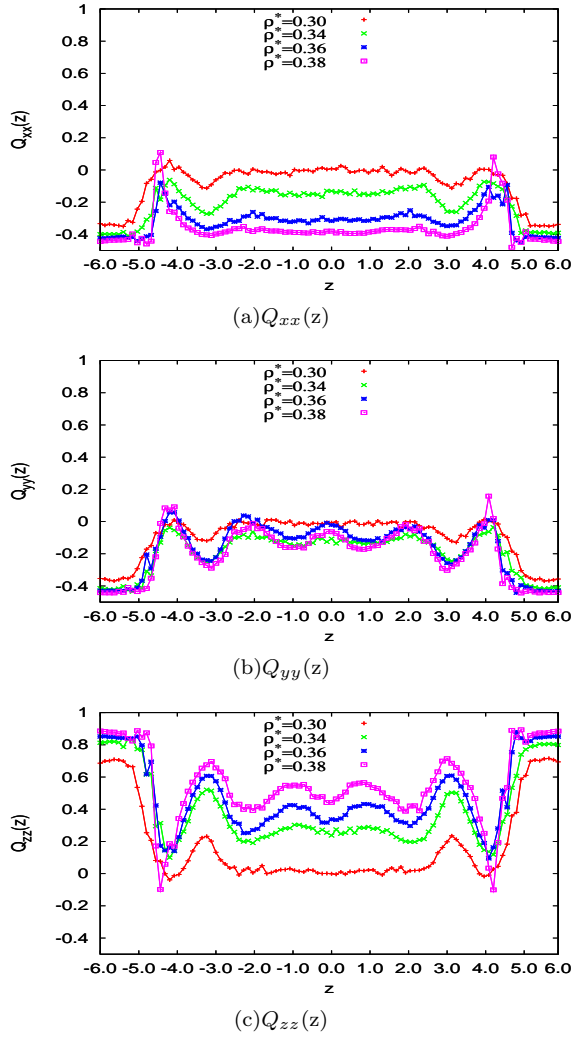


FIG. 6: (Color online) Density-dependent profiles of the diagonal components of the order tensor, homeotropic-confined region.

increased, Q_{yy} increases close to the wall (~ 0.9) as well as in the bulk (~ 0.5). This indicates that the average particle alignment has a significant component parallel to the y -axis. Correspondingly, Q_{zz} (Fig. 7(c)) is negative close to the walls, indicating that the surface particles lie in the plane of the substrate. As the density is increased, negative Q_{zz} values are also seen mid-film but these only go down to -0.2 . The implication of this combination of Q_{ii} behaviours is, again, that the molecules in the mid-film are tilted.

We can confirm these tilts by considering the off-diagonal components $Q_{xy}(z)$ and $Q_{xz}(z)$. The latter (not shown) are found to be zero at all densities. In Fig. 8, we show that the off-diagonal component $Q_{yz}(z)$ is also zero throughout the film for $\rho^* \leq 0.36$. For ρ^* greater than 0.36 , however $Q_{yz}(z)$ decreases and tends to -0.5 in both

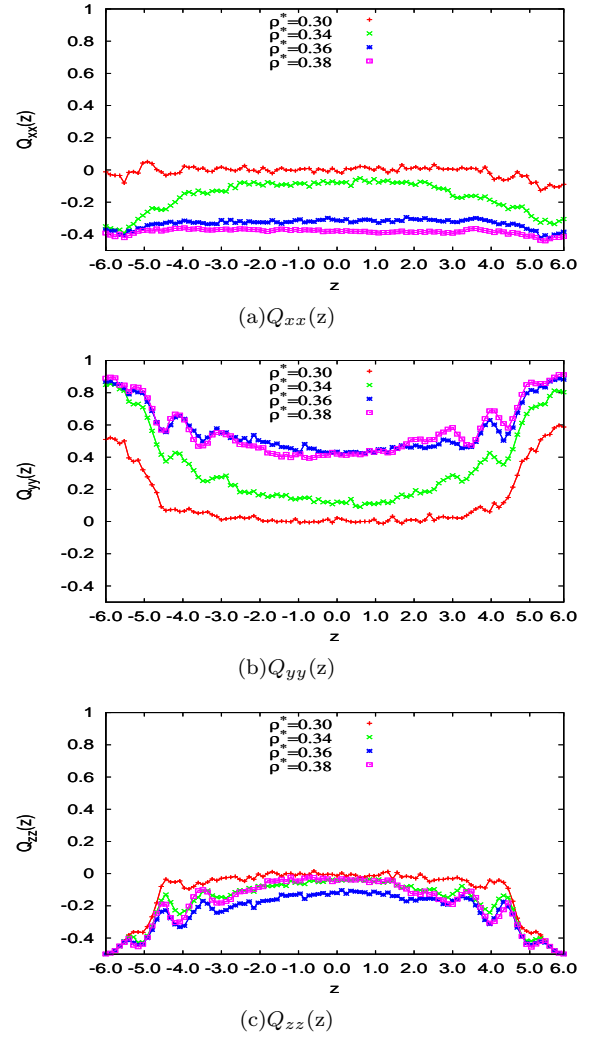


FIG. 7: (Color online) Density-dependent profiles of the diagonal components of the order tensor, planar-confined region.

the planar-confined and the homeotropic-confined portions.

In the light of this fuller analysis, we can now draw some conclusions concerning this initial stripe-patterned substrates system. Firstly, there is a strong tendency for the molecules to align in the plane of the stripe boundaries. Such behaviour has been seen experimentally in systems of LCs adsorbed at stripe-patterned substrates, e.g. [14]. We quantify this effect in Fig. 9, which shows the particle azimuthal-angle distribution function obtained at a reduced density of 0.39 . This is strongly peaked in the small azimuthal angle regime $0 \leq \phi \leq 5^\circ$.

The issue of polar anchoring is slightly more complex, however. At first sight, Figs. 3 suggest that the surface patterns are written unmodified across the film. However, the more detailed analysis given above shows that,

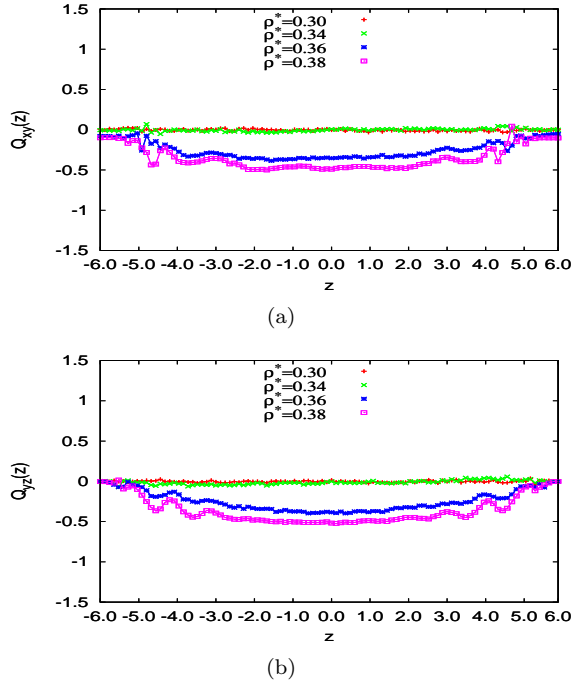


FIG. 8: (Color online) Density-dependent profiles of the off-diagonal component $Q_{yz}(z)$ of the order tensor for a) Homeotropic-confined region and b) planar-confined region.

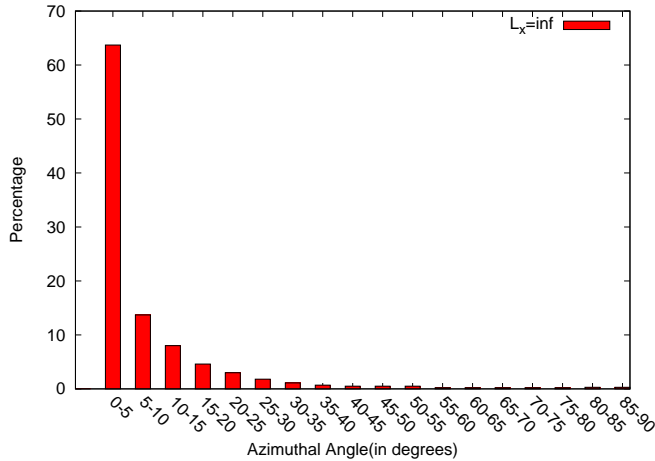


FIG. 9: (Color online) Histogram representing the particle azimuthal angle distribution in the planar surface region for the stripe patterned system with 50% H and 50% P coverage on the surfaces. $\rho^*=0.39$

in fact, the mid-film regions are tilted, a different tilt being observed between each surface-coupling region. From this, it is apparent that the two domains identified from Figs. 3 have a non negligible influence on one another. This leads to the mid-film director adopting a spatial variation in its y - and z -components, the x -component remaining small throughout. One can, alternatively, en-

visage the possibility of a uniformly oriented bulk monodomain being a stable arrangement. Such behaviour has been predicted previously at much larger length-scales by Kondrat *et al.*[20]. They considered LCs adsorbed at striped substrates with finite-strength homeotropic and homogeneous anchoring regions. Where one set of stripes was much narrower than the other, the bulk nematic was found to adopt a spatially uniform configuration rather than a periodically distorted arrangement. In the following sections, we investigate the requirements for this alternative scenario by considering the sensitivity of such systems to the relative surface coverage and the film thickness.

IV. INFLUENCE OF THE RELATIVE COVERAGE OF THE HOMEOTROPIC AND PLANAR SURFACE STRIPE REGIONS

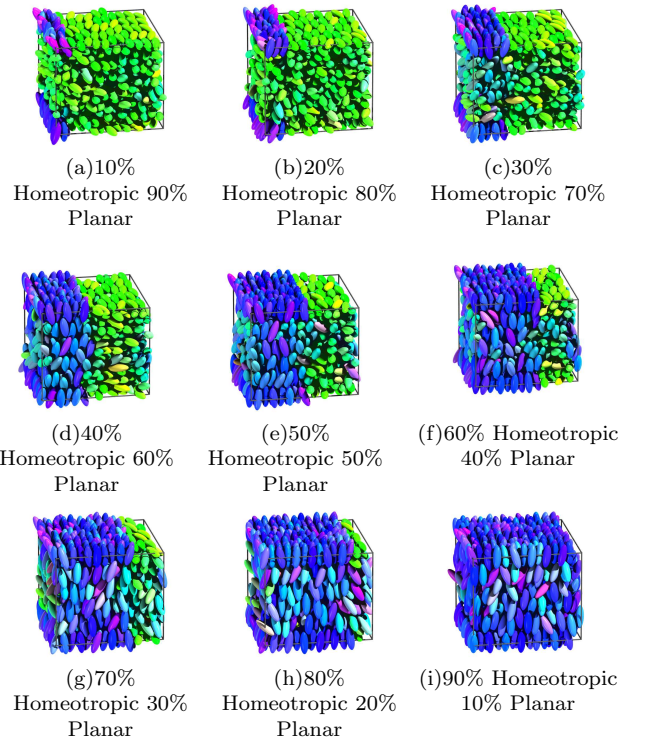


FIG. 10: (Color online) Snapshots of the stripe patterned system for different coverages of the homeotropic-confining and planar-confining substrate conditions). $\rho^*=0.4$

In this section, we assess the influence of the relative sizes of the homeotropic (H) and planar (P) striped alignment regions on the structure and anchoring of a confined LC film. To do this we present results from full compression sequences performed on a series of systems with substrate region coverages varying in 10% steps from 10% H, 90% P to 90% H, 10% P. In all other respects, these systems are identical to that described in the previous section. Figs. 10 present snapshots of the $\rho^*=0.4$ config-

urations obtained for this range of systems. These clearly indicate that, depending on the relative proportions of the homeotropic and planar substrate regions, these systems do, indeed, exhibit either a central monodomain or an alternating dual-domain bridging arrangement.

From these snapshots it appears that, for the proportions 10% H and 90% P (Fig. 10(a)), the mid-film part of the system is not significantly influenced by the presence of the homeotropic substrate region and the monodomain formed is equivalent to that of an unpatterned planar-aligned system. This observation also holds for the 20% H and 80% P system (Fig. 10(b)). It appears, then, that for this film thickness, the mid-film structure is insensitive to homeotropic alignment regions of less than $\simeq 30\%$. On the following snapshot (Fig. 10(c)), the system behaves differently. Here, the region confined between the $k_s=0$ surfaces *does* respond to the patterned substrate and the homeotropic alignment region forms a bridged domain across the film.

To substantiate this assessment, we plot, in Fig. 11, the mid-film region-averaged director orientation values θ_y and θ_z corresponding to the two substrate regions. At the limbs of this diagram, where the relative area proportions are poorly balanced, the angles observed coincide, indicating a mid-film monodomain arrangement. Here, the director field is distorted near to the substrates, but the central region forms a single domain whose orientation depends on the relative sizes of the homeotropic and homogeneous substrate regions. Note that for the 80% H system, for which the snapshot Fig. 10(h) suggests the thin planar-aligning surface strip has negligible influence, the mid-film anchoring angle is, in fact, tilted due to the substrate patterning. The alternative dual-domain-bridging arrangement, which occurs when the relative surface condition areas are more in balance, corresponds to systems in which the director angles differ in the two regions.

Importantly, the director angle trends observed here cover the full range from planar to homeotropic and, for each domain type, this anchoring angle appears to vary continuously with relative coverage proportion. Fig. 11, shows that the tilt angles vary monotonically as the relative stripe width is varied. This suggests that it may be possible to use stripe patterning to achieve *any* desired average director orientation in the mid-film region. Strong azimuthal alignment is found for all of these systems, the mid-film director alignments being effectively pinned to the y - z plane.

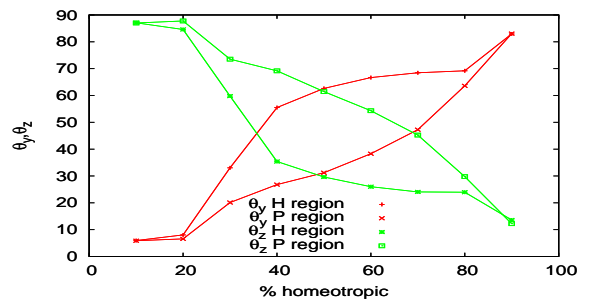


FIG. 11: (Color online) Comparison of θ_y and θ_z values in the two regions.

V. INFLUENCE OF THE THICKNESS OF THE LIQUID CRYSTAL FILM

In this section, we investigate the influence of film thickness on a relative stability of the single-domain and dual-bridged-domain structures observed in the previous section. We achieve this by considering three further 50% H, 50% P systems with substrate separations $6\kappa\sigma_0$, $7\kappa\sigma_0$ and $8\kappa\sigma_0$. These have been studied using compression sequences of simulations performed with system sizes of 1296, 1512 and 1728 particles, respectively. Other parameters and approaches have been held identical to those used in previous sections, such that, at each density considered, the surface areas of all systems were identical, with only the L_z values varying. High density snapshots corresponding to these plus the $4\kappa\sigma_0$ system described in section III are represented in Fig. 12. From these, we observe that, as L_z is increased, the domain bridging apparent in the thinnest film becomes increasingly diffuse. To quantify this further we again consider profiles calculated for the two differently confined portions of each system. Selected profiles for the $6\kappa\sigma_0$ and $8\kappa\sigma_0$ are shown in Figs. 13 and 14.

Comparing the Q_{zz} profiles corresponding to the homeotropic region, shown in Figs. 6(c), 13(a) and 14(a), we see that increasing L_z generally leads to a decrease in both the mid-film positional structure and the corresponding Q_{zz} value. Fig. 6(c), depicting the Q_{zz} profiles for the nominally homeotropic portion of the $L_z=4\kappa\sigma_0$ system, indicates clear formation of stratified layers both at the surfaces and in the mid-film region. At $\rho^*=0.39$, the average mid-film value of Q_{zz} is about 0.5. The formation of stratified layers is confirmed by the corresponding density profiles (Fig. 4(a)) which show that, away from the substrates, they are separated by a distance $\simeq 2.5\sigma_0$. As the thickness of the box is increased to $L_z=6\kappa\sigma_0$, the peaks in the homeotropic-region Q_{zz} profiles (Fig. 13(a)) become more damped near the centre of the film and the average mid-film value of $Q_{zz} \simeq 0.4$ at $\rho^*=0.4$. Looking at the corresponding density profile (Fig. 13(c)), we can see that there are now 7 discern-

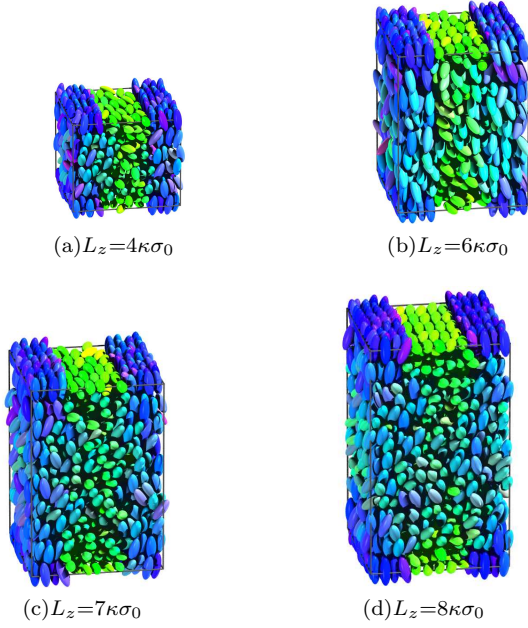


FIG. 12: (Color online) Snapshots of striped systems with different L_z values at $\rho^*=0.4$

able peaks in addition to the significant surface features. The distance between the surface monolayers and the second layers is $\simeq 3\sigma_0$, which corresponds to the particle length. The separation distance between subsequent layers is, however, decreased to $\simeq 2\sigma_0$. On increasing the film thickness further to $L_z=8\kappa\sigma_0$, the central region of the homeotropic-confined region loses all positional structure (Figs. 14(a) and 14(c)). At $\rho^*=0.39$, the latter shows 5 exponentially damped peaks at each wall. The corresponding Q_{zz} profile (Fig. 14(a)), shows behaviour characteristic of the onset of nematic ordering between densities $\rho^*=0.3$ and 0.34 , the average value of Q_{zz} rising to about 0.5 . However, with further increase in the reduced density to $\rho^*=0.36$, the mid-film Q_{zz} value *decreases* to an average of 0.25 and remains at that level at higher ρ^* .

Recalling the Q_{zz} profile for the planar-confined region of the $L_z=4\kappa\sigma_0$ system (Fig. 7(c)), we can see that its average mid-film value tends to -0.1 at high density. This departs markedly from the behaviour of an LC film confined between unpatterned $k_s=3$ substrates, which adopts planar orientations with $Q_{zz} \simeq -0.5$ [16]. As noted above, this difference arises due to the influence of the neighbouring homeotropic-confined regions. Unlike what was seen between the homeotropic-confining substrates, however, layering is restricted to the near-surface regions. On increasing the cell thickness to $L_z=6\kappa\sigma_0$, the mid-film Q_{zz} value becomes more negative for a density $\rho^*=0.34$ (Fig. 13(b)). This is close to the equivalent behaviour of a system confined between unpatterned planar-confining substrates. However, as the density is increased further to $\rho^*=0.36$, the mid-film Q_{zz} *increases*, rising to 0.1 and

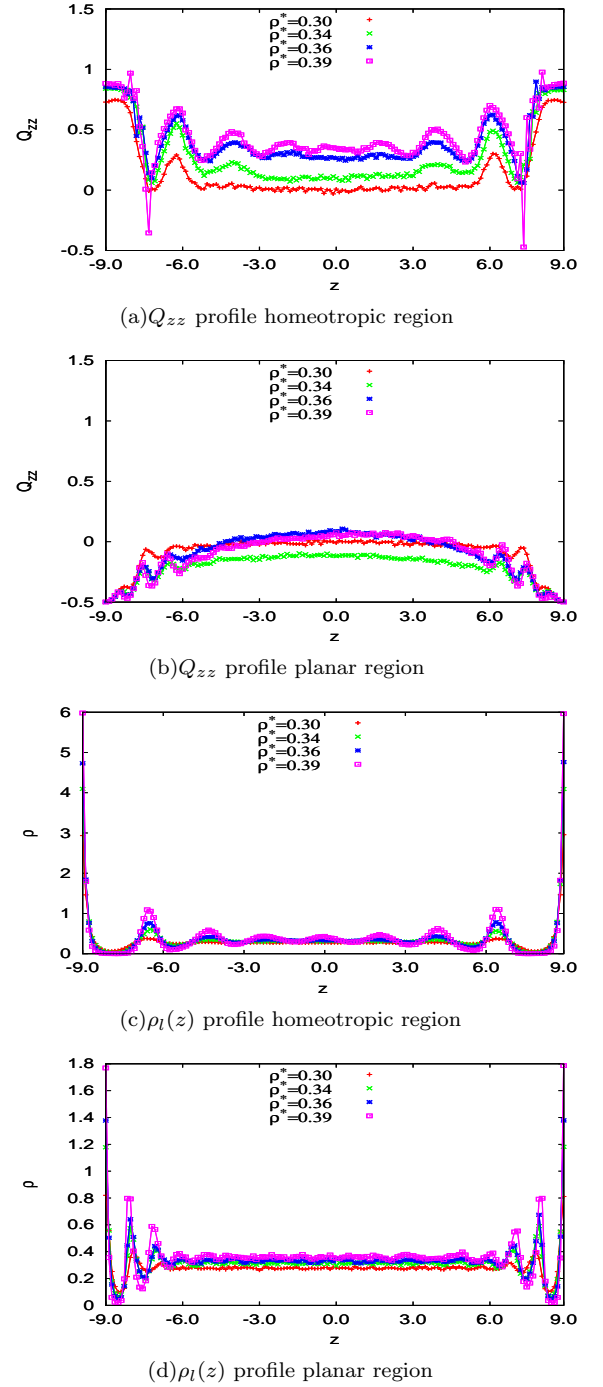


FIG. 13: (Color online) $L_z=6\kappa\sigma_0$: profiles corresponding to the two surface regions.

maintaining that value for $\rho^*=0.39$. For the thickest film considered here, alternative non-monotonic behaviour is observed. The Q_{zz} profiles in Fig. 14(b) show that, as the density is increased from 0.3 to 0.34 , despite the planar anchoring condition, the mid-film Q_{zz} value is $\simeq 0.4$. This is explained by the behaviour of the neighbouring homeotropic region: the mid-film Q_{zz} profiles for the two

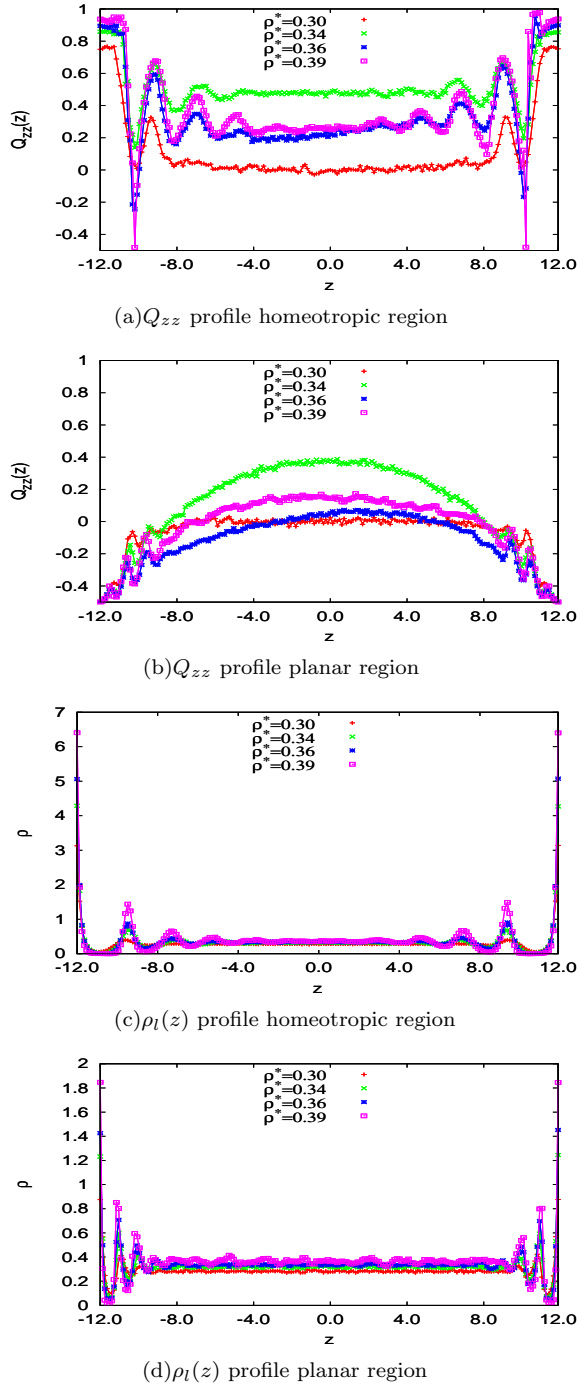


FIG. 14: (Color online) $L_z=8\kappa\sigma_0$: profiles corresponding to the two differently confined sub-systems.

differently confined regions (Figs. 14(a) and 14(b)) both attain this value, showing that the whole of the mid-film exhibits homeotropic anchoring at $\rho^*=0.34$. However, as the density is increased to 0.39, the two mid film regions both exhibit a drop in Q_{zz} value down to 0.1. This behaviour is similar to that seen by Bramble et al. [14] in which substrate-patterned systems are dominated by

homeotropic alignment at the nematic-isotropic transition, but are influenced by planar-aligning regions deeper into the nematic phase window.

To clarify the implications of these order tensor profile observations, we have calculated mid-film director orientations for the four film thicknesses studied. These are plotted in the high density limit in Fig. 15. This shows, unambiguously, that the high density $Q_{zz}(z)$ profiles for the thickest films correspond to the onset of significant mid-film director tilt. The mid-film tilt values obtained in the differently-confined regions are clearly different from one another for the thinnest film but converge as the film thickness is increased. This observation is in good agreement with the original inference from the snapshots Fig. 12 - increasing the film thickness leads to breakdown of the dual-bridged-domain arrangement in favour of a tilted central monodomain.

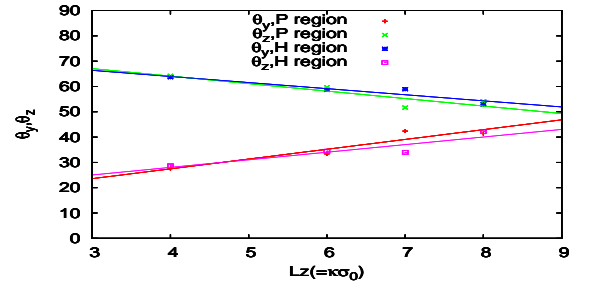


FIG. 15: (Color online) Variation of θ_y and θ_z in the homeotropically-confined (H) and planar-confined (P) regions for different film thicknesses L_z

VI. CONCLUSIONS

In this paper, we have presented a comprehensive simulation study of thin LC films confined between stripe-nanopatterned substrates. In these, we have concentrated on the influence of two parameters: the relative stripe width and the cell thickness. From this, we have shown that the relative stripe width is crucial in determining the polar anchoring behaviour exhibited in the mid-film region. Importantly, there appears to be a monotonic relationship between relative stripe width and bulk tilt angle. For very thin films, we have observed bridged domains of different orientation traversing the full film width. The orientations adopted by these domains have been shown to be partial tilts, adopted as a compromise between local substrate condition and neighbouring domain orientation. Increasing film thickness leads to a decay of this bridging arrangement, such that a single tilted monodomain becomes the dominant configuration. As a consequence, it appears clear that, provided the very thin film limit is avoided, tilted LC

monodomains with any desired polar anchoring angle can be obtained using systems of this geometry, the angle adopted being controlled by the relative stripe width. Stripe patterning imposes a strong azimuthal anchoring condition for all of the systems we have considered here.

Our studies of this class of system go beyond the data sets reported here. We can report, therefore, that while quantitative changes to system behaviour can be achieved by varying the surface coupling interactions, no qualitative changes are observed [21]. Further, we have found that the anchoring behaviour in these systems is generally insensitive to the nature of the patterning boundary used - essentially identical results are seen for sharp patterning boundaries (as used here) and diffuse boundaries. We *have* found that fundamentally different

behaviour can be observed in related systems based on 2-dimensional patternings such as squares and circles. We shall report on these in a future publication.

Acknowledgments

This work was supported by the Engineering and Physical Research Council, Grant No GR/S59833/01. We acknowledge useful conversations with Steve Evans, Jim Henderson, Jon Bramble, Chris Care, Tim Spencer and Paulo Teixeira which have been beneficial to our understanding of the systems studied here.

-
- [1] B. Jérôme, Reports on Progress in Physics **54**, 391 (1991).
 - [2] C. V. Brown, M. J. Towler, V. C. Hui and G. P. Bryan-Brown, Liquid Crystals **27**, 233 (2000).
 - [3] S. Kitson and A. Geisow, Applied Physics Letters **80**, 3635 (2002).
 - [4] J. H. Kim, M. Yoneya and H. Yokoyama, Nature **420** 159 (2002).
 - [5] D. W. Berreman, Physical review letters **28**, 1683 (1972).
 - [6] T. Z. Qian and P. Sheng, Physical Review E **55**, 7111 (1997).
 - [7] T. Z. Qian and P. Sheng, Physical Review Letters **77**, 4564 (1996).
 - [8] S. Park, C. Padeste, H. Schiff, J. Gobrecht and T. Scharf, Advanced Materials **17**, 1398 (2005).
 - [9] T. Scharf, S. Park, C. Padeste, H. Schiff, N. Basturk and J. Grupp, Molecular Crystals and Liquid Crystals **438**, 55/[1619] (2005).
 - [10] B. Lee and N. A. Clark, Science **291**, 2576 (2001).
 - [11] R. A. Drawhorn and N. L. Abbott, Journal Of Physical Chemistry **99** 16511 (1995).
 - [12] Y. L. Cheng, D. N. Batchelder, S. D. Evans, J. R. Henderson, J. E. Lydon and S. D. Ogier, Liquid Crystals **27** 1267 (2000).
 - [13] I. H. Bechtold and E. A. Oliveira, Liquid Crystals **32** 343 (2005).
 - [14] J. P. Bramble, S. D. Evans, J. R. Henderson, C. Anquetil, D. J. Cleaver and N. J. Smith, Liquid Crystals **34**, 1059 (2007).
 - [15] P. Padilla and E. Velasco, The Journal of Chemical Physics **106**, 10299 (1997).
 - [16] D. J. Cleaver and P. I. C. Teixeira, Chemical Physics Letters **338**, 1 (2001).
 - [17] F. Barmes and D. J. Cleaver, Physical Review E **69**, 061705 (2004).
 - [18] M. Schoen and D. J. Diestler, Chemical Physics Letters **270**, 339 (1997).
 - [19] M. Schoen, Physical Chemistry Chemical Physics **10**, 223 (2008).
 - [20] S. Kondrat, A. Poniewierski and L. Harnau, The European Physical Journal E **10**, 163 (2003).
 - [21] C. Anquetil-Deck, PhD Thesis : *Liquid crystal films confined between patterned substrates*, Sheffield Hallam University (2008).